

A Quadratic precision generalized nonlinear global optimization migration velocity inversion method*

Zhao Taiyin¹, Hu Guangmin¹, He Zhenhua², and Huang Deji²

Abstract: An important research topic for prospecting seismology is to provide a fast accurate velocity model from pre-stack depth migration. Aiming at such a problem, we propose a quadratic precision generalized nonlinear global optimization migration velocity inversion. First we discard the assumption that there is a linear relationship between residual depth and residual velocity and propose a velocity model correction equation with quadratic precision which enables the velocity model from each iteration to approach the real model as quickly as possible. Second, we use a generalized nonlinear inversion to get the global optimal velocity perturbation model to all traces. This method can expedite the convergence speed and also can decrease the probability of falling into a local minimum during inversion. The synthetic data and Marmousi data examples show that our method has a higher precision and needs only a few iterations and consequently enhances the practicability and accuracy of migration velocity analysis (MVA) in complex areas.

Keywords: Pre-stack depth migration, migration velocity analysis, generalized nonlinear inversion, common imaging gather.

Introduction

Pre-stack depth migration is regarded as an effective tool for obtaining accurate images in complex areas. With the development of migration theory and advancement of computer technology, an important research topic is the calculation of the pre-stack depth migration velocity model by applying pre-stack depth migration and achieving an accurate migrated section. The basic idea of this method is that when downward continuing to produce the migration depth image, we use two imaging conditions: zero time and zero offset. If the velocity model is correct, the two imaging conditions cooperate to produce a perfect seismic image. If the velocity model is incorrect, the zero offset and zero time conditions are inconsistent and a distorted seismic

image is produced. However, using this distorted seismic image, we can find the amount of distortion depending on the migration velocity and update the velocity model. After multiple iterations of pre-stack depth migration and velocity model updating, we can finally obtain an optimal migration velocity model. Presently, there are two types of pre-stack depth migration velocity analysis, depth focusing analysis (DFA) (MacKay and Abma, 1992; Wang and Pann, 1998; Liu et al, 2001, Liu et al., 2005) and residual velocity analysis (RVA) (Al-Yahya, 1989; Liu and Bleistein, 1995, Liu, 1997; Zhou et al, 2001; Biondi and Tisserant, 2004). Liu et al. (2005) and Liu and Wang (2006) demonstrated that event leveling in RVA is equivalent to equating imaging depth and focusing depth in DFA. In other words, these two methods constitutionally pursue the coherence of imaging and focusing depths. There are two questions

Manuscript received by the Editor December 15, 2008; revised manuscript received April 24, 2009.

*This work is supported by National Natural Science Foundation of China (Grant No.40839905).

1. School of Communication and Information Engineering, UESTC, Chengdu 610054, China.

2. State Key Laboratory of Oil and Gas Reservoir Geology and Exploitation, CDUT, Chengdu 610059, China

regarding the methods described above: (1) how to establish a criterion for determining if a migration velocity is acceptable and (2) how to update the velocity model if there are errors. Regarding the first question, DFA assumes that if the difference between migration depth and focusing depth equals zero, then the migration velocity is correct. RVA assumes that if the difference between traces with difference offsets is zero, then the migration velocity is correct. These two methods give essentially equivalent answers. As to the second problem, different pre-stack depth MVA methods deduce many velocity model correction methods, based on the criteria for the first question. A good approximation not only reduces the number of iterations but also increases the likelihood of convergence. Liu (1997) derived an analytical approach to MVA, which imposes no limitation on offset, dip, or velocity distribution. Meng et al. (1999a, 1999b) extended the analytical MVA method into 3-D. Liu et al. (2001) proposed a common image gather velocity analysis in the angle domain. Sava and Biondi (2004) advanced diffraction focusing velocity analysis. Liu and Wang (2006) proposed time shift depth focusing velocity analysis. Several problems exist with these methods: (1) Almost all existing MVA methods assume that there is a linear relationship between residual depth and residual velocity. This leads to a rough approximation to velocity since the equation for computing the velocity correction is only accurate to the first order. (2) While updating the velocity model, either fewer seismic gathers are used and analytical equations are used to calculate the new velocity model, which

cannot make sufficient use of all gather information in every pre-stack depth migration iteration; or a common optimal method is used, which cannot deduce a perfect velocity model correction. (3) If imaged depth picked from field data isn't accurate or there is some noise, the situation will become even worse. These factors require more iteration for the velocity model to converge to the correct one. Thus, these methods are hard to use in practice and restrict, not only the practicability of the MVA, but also the veracity of the imaging in complex structures.

In this paper, we propose a quadratic precision generalized nonlinear global optimization for migration velocity inversion. First, we discard the assumption that there is a linear relationship between residual depth and residual velocity and propose a velocity model correction equation with quadratic precision which enables every velocity model of every iteration to approach the real model as closely as possible. Second, by applying a generalized nonlinear inversion in pre-stack depth MVA, we advance a method for pre-stack depth migration-velocity inversion imaging. Such a method will not only reduce the number of inversion iterations, but also reduce the sensitivity to noise. The method effectively resolves problems (2) and (3) described above. The method proposed in this paper integrates pre-stack migration with migration velocity inversion, which can be used in complex media to get a precise velocity model and pre-stack depth migration section. We will discuss the theory, processing workflow, deduce the main equations, and give examples of synthetic and Marmousi data.

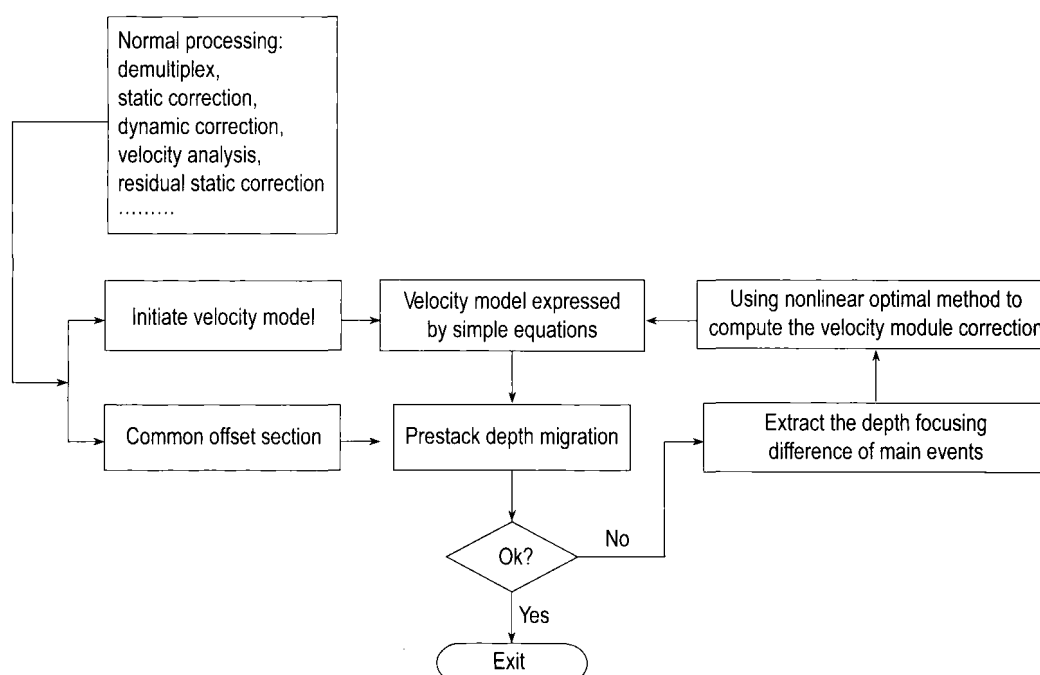


Fig. 1 The pre-stack depth migration velocity inversion procedure.

Pre-stack depth migration-velocity inversion imaging

Our technology idea is, first, based on RVA, to solve the problem described above, we discard the linear assumption and deduce a quadratic precision velocity model correction equation; and, second, we generate an initial velocity model consisting of many layers defined by different polynomials and variable velocity in both depth and lateral direction within each layer. The ultimate aim of migration velocity inversion is to obtain correct polynomials. In RVA, we construct a data gather from all traces associated with the same reflection layer. Then, we can acquire a globally optimal velocity model correction for all gathers using generalized nonlinear inversion. This approach is shown in Figure 1. The advantages of this procedure are: (1) we can use reflection information from all traces associated with the same reflection which not only improves the precision of each iteration but also reduce the sensitivity to noise. (2) Because using the quadratic velocity model correction equation which can improve the precision of every iteration, we are able to reduce the number of iterations. It is worth mentioning that because there are so many calculations in pre-stack depth migration, reducing the number of iterations is profoundly significant.

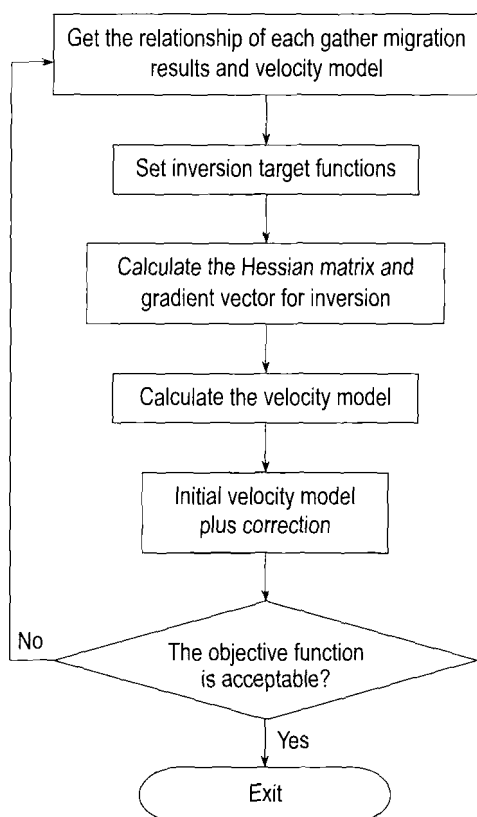


Fig.2 The flow chart for migration velocity inversion.

We use generalized nonlinear inversion for the following reasons: compared to linear inversion, generalized nonlinear inversion can achieve quadratic precision using the Taylor expansion in each iteration, greatly reducing the number of iterations. Although there is more computation required in each iteration, comparing with the normal computations of pre-stack depth migration, the workload is negligible. Besides, generalized nonlinear inversion has more advantages compared to linear optimization in the aspect of the solution space's properties, state, and stability. The flow chart for migration velocity inversion is shown in Figure 2.

Quadratic precision velocity model correction equation

After sorting the pre-stack gathers into common image gathers (CIGs), when migration velocity is correct, the imaged depths of individual imaged points at a CIG must be the same.

CIG imaging analysis

Considering the 2-D reflection geometry of the earth (see Figure 3), we denote a 2-D vector by x . Let $x_s = (x_s(\xi), z_s(\xi))$ be source positions and $x_r = (x_r(\xi), z_r(\xi))$ be receiver positions where ξ is the position parameter on the surface. For example, in common offset, ξ would be the midpoint of a source-receiver pair. In common shot, ξ would be a receiver location that is the distance from the fixed shot to the receiver. $\tau_s(x, x_s)$ denotes the travel time for the down-going wave from the shot point x_s to reflect point x . $\tau_r(x, x_r)$ denotes the travel time for an up-going wave from x to receiver point x_r . $t(\xi)$ is the total reflection travel time of both down-going and up-going waves:

$$\tau_s + \tau_r = t. \quad (1)$$

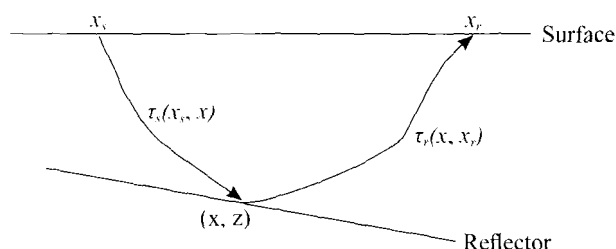


Fig. 3 2-D Reflection geometry.

The reflection point x is also a function of ξ and $x(\xi)$ satisfies Snell's law (Liu and Bleistein, 1995), which is expressed as

$$[\nabla_x \tau_s(x_s, x) + \nabla_x \tau_r(x, x_r)] \frac{dx}{d\xi} = 0. \quad (2)$$

From equation (2), we can get the imaging equation

$$\tau_s(x_s, x) + \tau_r(x, x_r) = t(\xi). \quad (3)$$

Taking the derivative of equation (3) gives

$$\frac{\partial \tau_s(x_s, x)}{\partial \xi} + \frac{\partial \tau_r(x, x_r)}{\partial \xi} = \frac{dt}{d\xi}. \quad (4)$$

Let $x_s = \text{constant}$, and $x_r = \xi + h$ where h is the offset from shot to receiver. In Figure 4, in the same CIG, we fix the horizontal coordinate of the reflection point x . The imaged depth z , the shot position x_s , the receiver position x_r , and parameter ξ can all be considered to be functions of the velocity c . That is, when the velocity changes, the migration imaging point at a particular trace location changes vertically. z is a function of migration velocity c . When x is kept unchanged, the image at the fixed x will come from different source-receiver pairs for different choices of c . That is, ξ is a function of c . We use the image equation (Liu and Bleistein, 1995):

$$\frac{dz}{dc} = \frac{z}{c \cos(\theta - \phi) \cos(\theta + \phi)}. \quad (5)$$

Equation (5) gives the quantitative relationship of migration image depth and migration velocity and it shows that the imaged depth increases with the migration velocity for fixed x , no matter what the true medium velocity is.

Linear velocity model correction equation

For a given migration velocity c and CIGs, let c^* denote the true medium velocity. When migration velocity $c = c^*$, the imaged depths of the same reflector at a CIG must be the same, i.e., z is independent of source-receiver pairs. With no loss of generality, we suppose that the source x_s is to the left of the receiver x_r , that is, the offset is bigger than 0. In the common shot case, different imaged traces in a CIG come from different shot gathers (see Figure 4).

$$x_s - x = -z \tan(\theta - \phi). \quad (6)$$

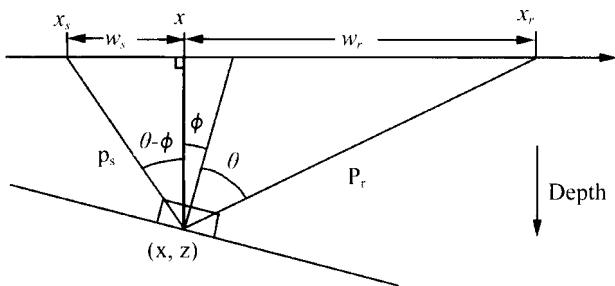


Fig.4 Raypath sketch where dip angle is ϕ and incidence angle is θ .

If we change the shot position, the equation (6) is derived with respect to x_s , let $c = c^*$, we have

$$\frac{d\theta}{dx_s} = -\frac{\cos^2(\theta - \phi)}{z} \Big|_{c=c^*}. \quad (7)$$

From Liu and Bleistein (1995), we have

$$\frac{\partial^2 z}{\partial x_s \partial c} \Big|_{c=c^*} = \frac{(x_s - x_r)P_r}{c^* z P_s}. \quad (8)$$

Expanding $\frac{\partial z}{\partial x_s}$ in $c = c^*$ with the Taylor expansion yields

$$\begin{aligned} \frac{\partial z}{\partial x_s} &\approx \frac{\partial z}{\partial x_s} \Big|_{c=c^*} + \frac{\partial^2 z}{\partial x_s \partial c} \Big|_{c=c^*} (c - c^*) \\ &= \frac{(x_s - x_r)P_r (c - c^*)}{c^* z P_s}, \end{aligned} \quad (9)$$

where

$$P_s = \sqrt{(x_s - x)^2 + z^2}, \quad P_r = \sqrt{(x_r - x)^2 + z^2}.$$

Suppose that we have two shots: x_{s1} , x_{s2} , and $x_{s1} < x_{s2}$. Then the difference in imaged depths between these two shots at a CIG can be approximated by

$$z(x_{s2}) - z(x_{s1}) \approx (x_{s2} - x_{s1}) \frac{(c - c^*)}{c^* z} \frac{P_r}{P_s}, \quad (10)$$

where $x_{s0} = (x_{s1} + x_{s2})/2$ and x_{s0} is the corresponding receiver position. Thus, we find

$$\frac{c - c^*}{c^*} = \frac{\Delta z \cdot z}{\Delta x_s (x_{s0} - x_{r0})} \frac{P_s}{P_r}, \quad (11)$$

where $\Delta x_s = x_{s2} - x_{s1}$ and $\Delta z = z(x_{s2}) - z(x_{s1})$.

Quadratic precision velocity model correction equation

To improve the correction equation precision, expand $\frac{\partial z}{\partial x_s}$ at $c = c^*$, with the Taylor expansion to second-order accuracy, yielding

$$\frac{\partial z}{\partial x_s} \approx \frac{\partial z}{\partial x_s} \Big|_{c=c^*} + \frac{\partial^2 z}{\partial x_s \partial c} \Big|_{c=c^*} (c - c^*) + \frac{\partial^3 z}{\partial x_s \partial c^2} \Big|_{c=c^*} (c - c^*)^2, \quad (12)$$

Let

$$\begin{aligned} D_0 &= 2 \left(\frac{(z^2 - w_s w_r)P_r}{z c^* P_s^3} + \frac{P_r (x_r - x_s)^2}{z c^* P_s^3} - \frac{P_r w_s (x_r - x_s)}{c^* z P_s^3} \right), \\ D_1 &= -\frac{2}{c^*} \left(\frac{(z^2 - w_s w_r)P_r}{z c^* P_s^3} + \frac{P_r (x_r - x_s)^2}{z c^* P_s^3} \right. \\ &\quad \left. - \frac{P_r w_s (x_r - x_s)}{c^* z P_s^3} \right) \left(1 - \frac{P_s P_r}{z^2} \right) \end{aligned}$$

Nonlinear global optimization migration velocity inversion

$$D_2 = 2 \frac{P_r^2 (x_r - x_s)^2}{c^{*2} z^4} + 2 \frac{P_s P_r}{c z^2} \left(\frac{(z^2 - w_s w_r) P_r}{z c^* P_s^3} \right. \\ \left. + \frac{P_r (x_r - x_s)^2}{z c^* P_s^3} - \frac{P_r w_s (x_r - x_s)}{c^* z P_s^3} \right) \\ D_3 = \frac{1}{c^{*2} z^3} \frac{(x_r - x_s)^2 P_r^2}{P_s^2}. \quad (13)$$

From Appendix A, we have

$$\frac{\partial^2 z}{\partial x_s^2} \approx D_0 (c - c^*) + (D_1 + D_2 + D_3) (c - c^*)^2. \quad (14)$$

Suppose that we have three shots x_{s1} , x_{s2} , and x_{s3} and $x_{s1} < x_{s2} < x_{s3}$, the imaged depth difference in CIGs can be approximated by

$$\frac{\partial z(x_{s23})}{\partial x_s} - \frac{\partial z(x_{s12})}{\partial x_s} \approx \frac{\partial^2 z(x_{s13})}{\partial x_s^2} (x_{s3} - x_{s1}) / 2, \quad (15)$$

$$\frac{z(x_{s3}) - z(x_{s2})}{x_{s3} - x_{s2}} - \frac{z(x_{s2}) - z(x_{s1})}{x_{s2} - x_{s1}} \approx \frac{\partial^2 z(x_{s13})}{\partial x_s^2} (x_{s3} - x_{s1}) / 2, \quad (16)$$

where

$$x_{s12} = (x_{s1} + x_{s2}) / 2, x_{s23} = (x_{s2} + x_{s3}) / 2,$$

and

$$x_{s13} = (x_{s3} + x_{s1}) / 2.$$

Using equation (14), equation (16) becomes

$$2 \left(\frac{z(x_{s3}) - z(x_{s2})}{x_{s3} - x_{s2}} - \frac{z(x_{s2}) - z(x_{s1})}{x_{s2} - x_{s1}} \right) / (x_{s3} - x_{s1}) \\ \approx D_0 (c - c^*) + (D_1 + D_2 + D_3) (c - c^*)^2, \quad (17)$$

Let

$$A_2 = D_1 + D_2 + D_3,$$

$$A_1 = D_0,$$

and

$$A_0 = 2 \left(\frac{z(x_{s3}) - z(x_{s2})}{x_{s3} - x_{s2}} - \frac{z(x_{s2}) - z(x_{s1})}{x_{s2} - x_{s1}} \right) / (x_{s3} - x_{s1}). \quad (18)$$

We have

$$A_0 = A_1 (c - c^*) + A_2 (c - c^*)^2. \quad (19)$$

Equation (19) is the quadratic precision velocity model correction equation that we wanted (the particular derivation is shown in Appendix A). On the face of it, equation (19) is much more complex than the linear equation and the velocity model correction solution is not very direct. However, the added computations in equation (19) are mainly simple calculations and the increased computation is acceptable. Considering the

enhanced computation precision, which may decrease the number of pre-stack migration iterations, is well worth the computation increase.

Migration velocity generalized nonlinear inversion

Based on equation (19) and using only the CIG and its k neighboring traces, where k is equal to three times of the number of unknown quantities in the velocity function, we can calculate the velocity model correction. In fact, since each CIG usually has several traces, normally equal to the fold, plus the traces neighboring to this CIG, the number of traces of each layer is far larger than k . Because of existing error of the seismic data, if we combined every set of k traces and then use equation (19) to calculate the velocity model correction, we may not get identical results and may even get additional errors. We also cannot get the same velocity model correction by using the neighboring CIGs. At times, abrupt changes appear in the horizontal direction which are irregular and do not correspond to real geological conditions. Such velocity model corrections have low precision and high noise sensitivity, which significantly influences practical use of the method. To resolve such problems, we first parameterize the velocity model. In other words, we use a set of relatively simple functions to describe the layer velocity, which may have both horizontal and vertical velocity variation. Then using the generalized nonlinear inversion method and the quadratic precision velocity correction equation, we calculate the corrections of the unknown quantities in velocity model or invert the globally optimal velocity model correction.

The problems of migration velocity inversion

Traditional pre-stack depth MVA usually supposes that the velocity in a layer is constant, which does not accord with reality. If we want the inversion of the velocity model to vary in both horizontal and vertical directions, there are so many unknown quantities that the inversion becomes unstable or difficult to converge. However, for a given layer, the horizontal and vertical velocity variations are not fully disordered or irregular. So, we can assume that the lateral and vertical velocity variation can be approximated by a simple function for a given layer.

For example, let the velocity be a linear or second-order function of abscissa x and depth z ,

$$v(x, z) = \alpha_0 + \alpha_1 x + \alpha_2 z + \alpha_3 xz + \alpha_4 x^2 + \alpha_5 z^2, \quad (20)$$

or be a linear or second-order function of abscissa x ,

$$v(x, z) = \alpha_0 + \alpha_1 x + \alpha_4 x^2. \quad (21)$$

Thus, for a given layer, we only need to solve for the six parameters $\alpha_0, \alpha_1, \alpha_2, \alpha_3, \alpha_4, \alpha_5$ or the three parameters $\alpha_0, \alpha_1, \alpha_4$, which not only decreases the number of unknown quantities and enhances the speed, stability, and convergence of the inversion, but ensures a reasonable precision.

The derivation in this paper is based on a given layer, whereas real subsurface media can be divided into a number of layers. In such multi-layer media, it is theoretically possible to get a correction equation for the velocity model with large offset, steep dip, and horizontally variable velocity. Such a procedure is too complex to use in practice. To calculate the migration velocity of each layer, we usually use a method called layer-stripping to calculate the velocity in each layer one by one. In each layer, two initial velocity guesses are used: one is larger than the true layer velocity and the other one is smaller than the true layer velocity. We set the final velocity model correction as a weighted interpolation of these two models' correction. The weights are measured from the difference of the imaged points' horizontal location in the CIG. In velocity inversion, we use the layer-stripping method, processing operators with experience are needed to ascertain the time position between these layers, get the layer velocity by inversion, and then calculate the layer thicknesses.

The theory of migration velocity generalized nonlinear inversion

Suppose there are m CIGs in a given interface and there are n traces in each CIG. When the migration velocity is incorrect, suppose the real velocity model correction is σ . Let $\sigma = c - c^*$, $\sigma = \alpha_0 + \alpha_1 x + \alpha_2 z + \alpha_3 xz + \alpha_4 x^2 + \alpha_5 z^2$ and $\bar{\lambda} = [\alpha_0, \alpha_1, \dots, \alpha_5]^T$. The n traces of each CIG are from different shot gathers, among which, every three traces can form an imaged group and n traces of each CIG can make up $n-2$ imaged groups independent of each other. There is a total of $l = m(n-2)$ independent imaged groups. For every imaged group, $A_{0,i} A_{1,i} A_{2,i}$ is not the same and can be denoted by A_0, A_1, A_2 ($i = 1 \dots l$) where x, z is denoted by x_i, z_i ($i = 1 \dots l$).

In MVA, the calculated velocity model corrections based on different imaged groups may be different. We introduce the generalized nonlinear inversion method with the aim to acquire an optimal velocity model correction. Therefore, we form the objective function:

$$f(\bar{\lambda}) = \sum_{i=1}^l \|A_{0,i} - A_{1,i}\sigma - A_{2,i}\sigma^2\|$$

$$= \sum_{i=1}^l (A_{0,i} - A_{1,i}\sigma - A_{2,i}\sigma^2)^2 \rightarrow \min. \quad (22)$$

We expand the objective function at $\bar{\lambda} = \bar{\lambda}_0$ by using Taylor series

$$f(\bar{\lambda}_0 + \Delta\bar{\lambda}) = q(\Delta\bar{\lambda}) = f(\bar{\lambda}_0) + \bar{g}(\bar{\lambda}_0)\Delta\bar{\lambda} + \frac{1}{2}\Delta\bar{\lambda}H(\bar{\lambda}_0)\Delta\bar{\lambda}$$

where $\bar{g}(\bar{\lambda}_0) = \nabla f(\bar{\lambda}_0)$ is the gradient vector of $f(\bar{\lambda}_0)$ at $\bar{\lambda}_0$ and $H(\bar{\lambda}_0) = \nabla^2 f(\bar{\lambda}_0)$ is Hessian matrix of $f(\bar{\lambda}_0)$ at $\bar{\lambda}_0$. If the matrix H is symmetrical and positive definite, there must be minimize points for $q(\Delta\bar{\lambda})$.

Differentiating with respect to $\Delta\bar{\lambda}$ in the equation, we get

$$\frac{\partial f(\bar{\lambda}_0 + \Delta\bar{\lambda})}{\partial \Delta\bar{\lambda}} = \bar{g}(\bar{\lambda}_0) + H\Delta\bar{\lambda} = 0,$$

Then we can get $\Delta\bar{\lambda} = -H^{-1}\bar{g}(\bar{\lambda}_0)$. Let $\lambda = \lambda_0 + \Delta\lambda$. $\bar{\lambda}$ denotes the initial guess and repeat the procedure until $\|\Delta\bar{\lambda}\| < \varepsilon$ where ε is a given positive constant before inversion. We believe that $\bar{\lambda}$ at this time is the optimal estimated solution.

The gradient vector is:

$$\bar{g} = [g_0, g_1, \dots, g_5], \quad (23)$$

$$g_i = \sum_{j=1}^l 2(A_{0,j} - A_{1,j}\sigma - A_{2,j}\sigma^2) \cdot (2A_{2,j}\sigma + A_{1,j}) \frac{\partial \sigma}{\partial \alpha_i}, \quad (24)$$

$$\frac{\partial \sigma}{\partial \alpha_i} = \begin{cases} 0 & i = 0 \\ x_i & i = 1 \\ z_i & i = 2 \\ x_i z_i & i = 3 \\ x_i^2 & i = 4 \\ z_i^2 & i = 5 \end{cases}, \quad (25)$$

and the Hessian matrix is:

$$H = [h_{ik}]_{6 \times 6}, \quad (26)$$

$$h_{ik} = \frac{\partial g_i}{\partial \alpha_k}$$

$$= \sum_{j=1}^l -2 \frac{\partial \sigma}{\partial \alpha_i} \frac{\partial \sigma}{\partial \alpha_k} (-6A_{2,j}^2\sigma^2 - 6A_{1,j}A_{2,j}\sigma + 2A_{0,j}A_{2,j} - A_{1,j}^2).$$

$$(27)$$

Examples of synthetic and Marmousi models

The derivation of the quadratic precision velocity

Nonlinear global optimization migration velocity inversion

model correction equation is not based on the assumption that there is a linear relationship between residual depth and residual velocity. We also propose the new method using generalized nonlinear inversion to analyze the CIGs migration velocity. To validate these methods, we test using synthetic data and the Marmousi model.

Testing the ability of noise sensitivity

To validate the method's adaptability for the cases of horizontal and vertical velocity changes within a layer and the method's capability for noise reduction, we designed the geological model shown in Figure 5. In the first layer, velocity changes horizontally but is constant in depth. In the second layer, velocity changes both horizontally and vertically. We assume that the reflection time from the second layer has a 3% random error. The synthetic seismogram is shown in Figure 6. We only show two shots in the figure and each shot has 72 traces. In the first layer, the initial two velocity guesses are $V = 700.0 + 1.0x$ m/s (smaller than the true velocity) and $V = 1000.0 + 3.5x$ m/s (bigger than the true velocity). After one iteration of pre-stack depth migration-velocity

model correction procedure, we get an estimated first layer velocity of $V = 809.97 + 2.47x$. In the second layer, the two initial velocity guesses are $V = 600.0 + 1.0x + 2.0z$ m/s (smaller than the true velocity) and $V = 1200.0 + 2.5x + 5.0z$ m/s (bigger than the true velocity). After two iterations of pre-stack depth migration-velocity model correction, we get an estimated second layer velocity of $V = 958.97 + 1.63x + 3.85y$. The estimated velocity model is shown in Figure 7. We can get the final acceptable velocity model using only one iteration of pre-stack depth migration-velocity model correction. If the exit criterion is not met, it is necessary to use two iterations. From the inversion results we can get the following conclusion: for the three velocity function parameters, the part of the model where the layer velocity is constant has the highest precision; the part of the model with the velocity changing horizontally has an intermediate precision; and the part of the model with velocity changing in depth has comparatively lower precision. However, the error is smaller than 1.5% overall. Using the estimated velocity in pre-stack depth migration, we get the final migrated image, shown in Figure 8.

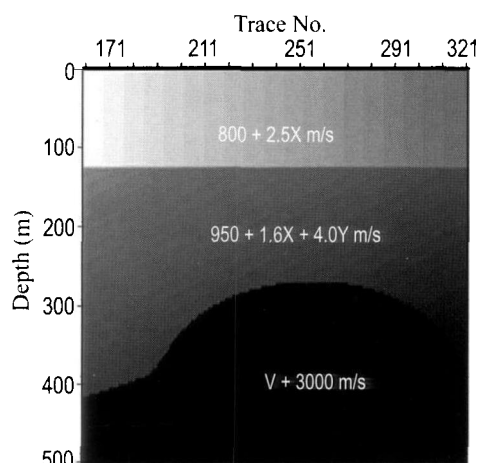


Fig. 5 Synthetic model in which the velocity changes horizontally and vertically.

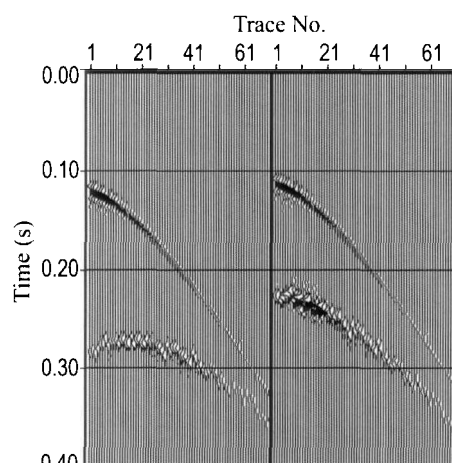


Fig. 6 Two common shot gathers of the model in Figure 5.

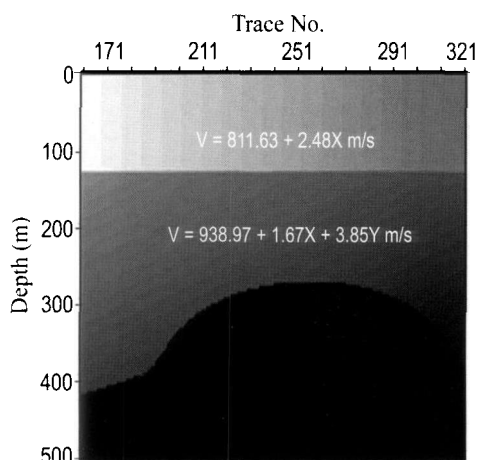


Fig. 7 Velocity model obtained by the inversion.

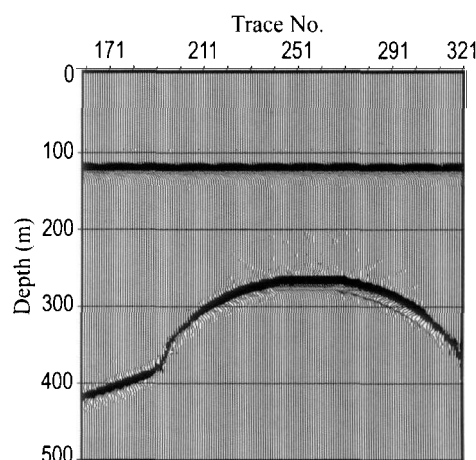


Fig. 8 The migrated section result.

Marmousi model test

We use Marmousi model data to verify the validity of our method for imaging complex structure. The Marmousi model contains many reflectors, steep dips, and strong horizontal and vertical velocity variations. The minimum velocity is 1500 m/s and the maximum

velocity is 5500 m/s. The actual velocity model is shown in Figure 9. The Marmousi data set contains 240 shot gathers with each shot including 96 receiver traces. For the sake of speed computation, for velocity analysis we selected 48 receiver gathers to analyze for each shot.

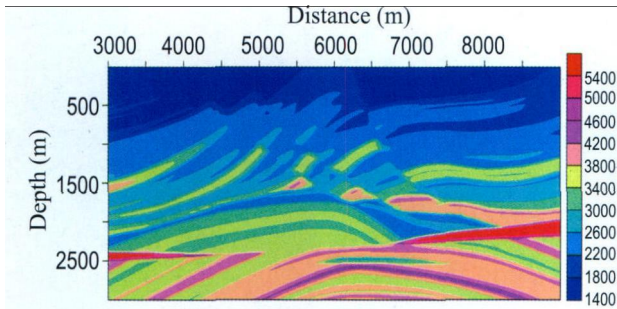


Fig. 9 The actual Marmousi velocity model.

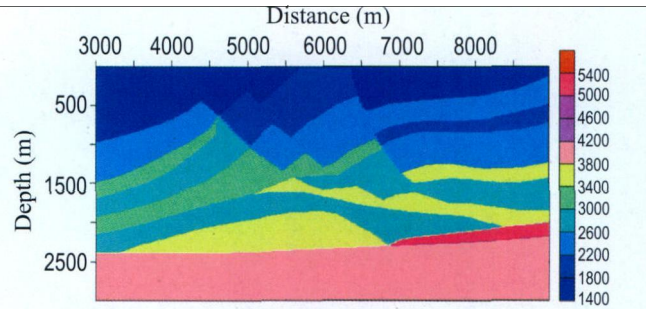


Fig.10 The estimated Marmousi velocity model.

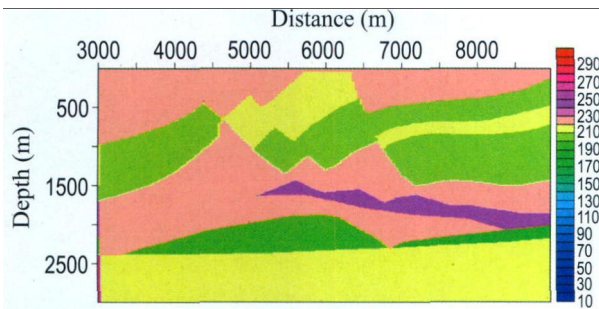


Fig.11 The residual velocity section.

For computation convenience, we assume that the velocity model consists of many models (i.e. contains many velocity layers) and for each layer the velocity is a linear function of x (abscissa) and z (depth), that is, $v(x,z) = \alpha_0 + \alpha_1 x + \alpha_2 z$. In order to enhance migration imaging precision and reduce the number of iterations, we used extended local Rytov Fourier migration (Huang

et al., 1999). After one or two pre-stack depth migration-velocity model correction iterations for every layer, we get the final velocity model which is shown in Figure 10. The residual velocity section is shown in Figure 11, which comes from the actual and estimated velocity models. In each layer of the residual velocity section, we averaged the absolute difference of the actual and estimated velocity models. Though the estimated velocity is not the same as the true model, it matches well not only in structure but also the velocity values. The migrated section using the estimated velocity model (Figure 10) and Marmousi data is shown in Figure 12. The migrated section using the actual velocity is shown in Figure 13. Comparing these two results, we can deduce that the migrated section using the estimated velocity model gives an acceptable structural image, which indicates the capability of our MVA approach for handling complex structures.

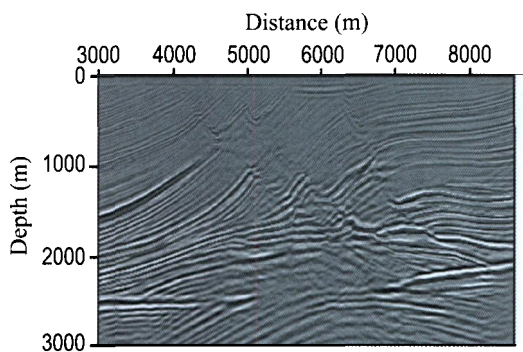


Fig.12 The Marmousi pre-stack migrated section using the estimated velocity model.

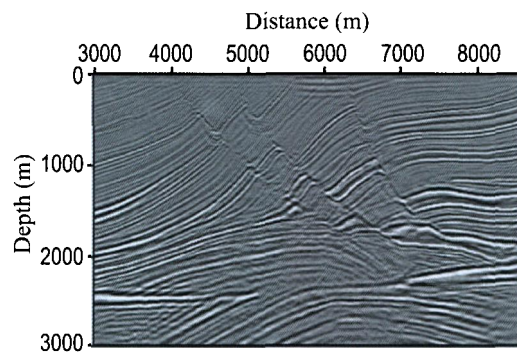


Fig.13 The Marmousi prestack migrated section using the actual velocity model.

The common image gathers selected from migrated data are shown in Figures 14 and 15. The CIGs in Figure 14 are migrated using the initiate velocity module. In Figure 14 (a), the image location ranges from 5000 m to

5120 m and in Figure 14 (b) it ranges from 7000 meter to 7120 meter. The CIGs in Figure 15 are migrated using the corrected velocity module; the image location is the same as Figure 14.

Conclusions

We can deduce following conclusions by the theoretical analysis and the quadratic precision generalized nonlinear migration velocity inversion results of the theoretical model:

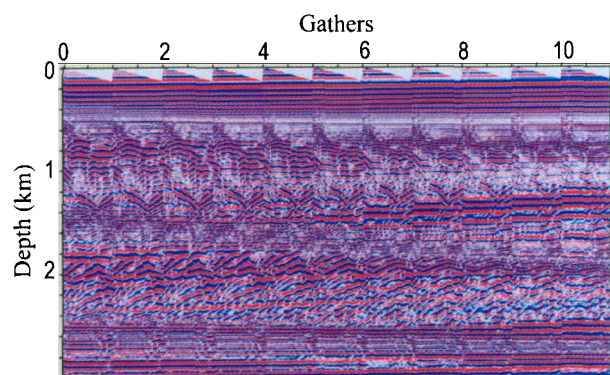
(1) By applying generalized nonlinear inversion into the calculation of the velocity model corrections, we are able to use the reflection information of all traces associated with same reflection layer. Therefore, we can not only resolve the problem that the velocity model correction equation is too complex to compute directly but also improve the precision of every iteration and reduce the sensitivity to noise.

(2) Compared to the linear equation, the quadratic precision velocity model correction equation discards the assumption that there is a linear relationship between residual depth and residual velocity. This method expedites the convergence speed greatly (usually it only needs one or two iterations for each velocity layer to achieve acceptable results, whereas two to four iterations are required in normal linear correction equations). Because the main computations in pre-stack depth migration are in the iterations of pre-stack depth migration, our method can expedite the process of MVA.

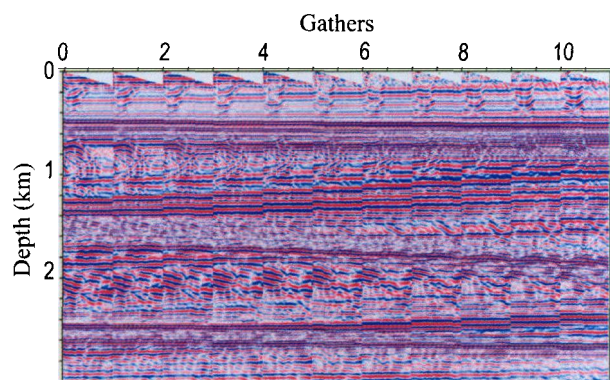
(3) Utilizing the method of generalized nonlinear inversion, we can achieve Taylor series quadratic precision in the iterations. This greatly expedites the convergence speed and decreases the probability of falling into a local minimum in the inversion processing.

References

- Al-Yahya, K., 1989, Velocity analysis by iterative profile migration: *Geophysics*, **54**, 718 – 729.
- Biondi, B., and Sava, P., 1999, Wave-equation migration velocity analysis: 69th Ann. Internat. Mtg., Soc. Expl. Geophys., Expanded Abstracts, 1723 – 1726.
- Biondi, B., and T. Tisserant, 2004, 3-D angle-domain common-image gathers for migration velocity analysis: *Geophysical Prospecting*, **52**, 575 – 591.
- Guo, J. Y., and Zhou, H. B., 2002, Toward accurate velocity models by 3D tomographic velocity analysis: EAGE 64th Conference & Exhibition, 27 – 30.

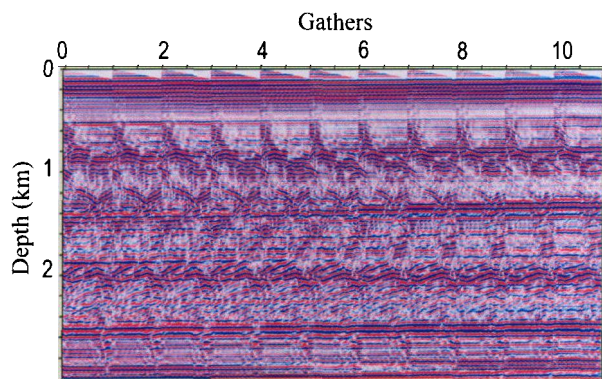


(a) The image location ranges from 5000 meter to 5120 meter.

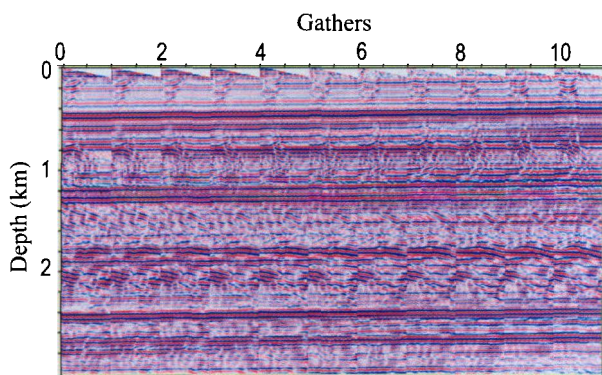


(b) The image location ranges from 7000 meter to 7120 meter.

Fig.14 Eleven CIGs from migrated data using the initiate velocity module. Forty traces are selected in each CIG module.



(a) The image location ranges from 5000 m to 5120 m;



(b) The image location ranges from 7000 m to 7120 m.

Fig.15 Eleven CIGs from migrated data using the corrected velocity. Forty traces are selected in each CIG.

- He, Z. H., Huang, D. J., and Hu, G. M., 1999, The characteristic, theory and its application of seismic wave field in complex oil-gas reservoir: Sichuan Publishing House of Science & Technology.
- He Z. H., 1989, Seismic reflection data migration and inverse methods, Chongqing Publishing House.
- He, Z. H., Xiong, G. J., and Zhang, Y. X., 1998, Nonzero offset seismic forward modeling by one-way acoustic wave equation: 68th Ann. Internat. Mtg., Soc. Expl. Geophys., Expanded Abstracts, 1921 – 1924.
- Hu, G. M., He, Z. H., and Huang, D. J., 2001, Nonlinear optimal inversion of seismic trace: Chinese Journal of Geophysics, **44**, 240 – 247.
- Huang, L. J., Fehler, M., and Roberts, P., 1999, Extended local Rytov Fourier migration method, Geophysics, **64**(1), 1524 – 1534.
- Huang, L. J., Fehler, M., and Wu, R.S., 1999, Extended local Born Fourier migration method, Geophysics, **64**(1), 1535 – 1545.
- Lafond, C. F., and Levander, A. R., 1993, Migration moveout analysis and depth focusing: Geophysics, **58**(1), 91 – 100.
- Li, Y. M., 2002, Improving the level of seismic wave's migration and attribute's description in face of exploration and exploitation: Progress in Exploration Geophysics, **17**(2), 198 – 210.
- Liu, S. W., and Wang, H. Z., 2006, Time-shift depth-focusing for migration velocity analysis: Internat. Geophy. Mtg., SPG/SEG. Expanded Abstracts, 51 – 54.
- Liu, S. W., Geng, J. H., Feng, W., 2005, Controlled illumination and seismic acquisition geometry for target-oriented imaging: Applied Geophysics, **2**(4), 230 – 234.
- Liu, W., Popovici, A. M., and Bevc, D., 2001, 3D migration velocity analysis for common image gathers in the reflection angle domain: 71th Ann. Internat. Mtg., Soc. Expl. Geophys., Expanded Abstracts, 885 – 888.
- Liu, Z. Y., and Bleistein, N., 1995, Migration velocity analysis: Theory and an iterative algorithm: Geophysics, **60**(1), 142 – 153.
- Liu, Z. Y., 1997, An analytical approach to migration velocity analysis: Geophysics, **62**(4), 1238 – 1249.
- Mackay, S. and Abma, R., 1992, Imaging and velocity estimation with depth-focusing analysis: Geophysics, **57**(6), 1608 – 1622.
- Meng, Z. B., Bleistein, N., and Waytt, K., 1999a, 3-D analytical migration velocity analysis I: Two-step velocity estimation by reflector-normal update: 69th Annual Internat. Mtg., Soc. Expl. Geophys., Expanded Abstracts, 1727 – 1730.
- Meng, Z. B., Bleistein, N., and Valasek, P., 1999b, 3-D analytical migration velocity analysis II: Velocity gradient estimation: 69th Annual Internat. Mtg., Soc. Expl. Geophys., Expanded Abstracts, 1731 – 1734.
- Sava, P., and Biondi, B., 2004, Diffraction-focusing migration velocity analysis: 74th Ann. Internat. Mtg., Soc. Expl. Geophys., Expanded Abstracts, 2395-2398.
- Schuster, G. T., and Hu, J. X., 2000, Green's function for migration: Continuous recording geometry: Geophysics, **65**(1), 167 – 175.
- Wang, B., and Pann, K., 1998, Model-based interpretation of focusing panels for depth focusing analysis: 68th Ann. Internat. Mtg., Soc. Expl. Geophys., Expanded Abstracts, 1596 – 1599.
- Xin, K. F., Wang, H. Z., and Ma, Z. T., 2002, Migration + inversion: An accurate migration velocity analysis method: Progress in Exploration Geophysics, **25**(3), 20 – 26.
- Yang, W. C., 1989, Geophysical inversion and the seismic CT method: Geological Publishing House.
- Zhang, W. S., and Zhang, G. Q., 2001, Prestack depth migration by hybrid method with high precision and its parallel implementation: Chinese Journal of Geophysics, **44**(4), 542 – 551.
- Zhou, H. B., Guo, J. Y., and Young, J., 2001, An alternative residual-curvature velocity updating method for prestack depth migration: 71th Ann. Internat. Mtg., Soc. Expl. Geophys., Expanded Abstracts, 877 – 880.

Appendix

The deduction of the quadratic velocity model correction equation

Expanding $\frac{\partial z}{\partial x_s}$ at $c=c^*$ with the Taylor series to second order accuracy, yields

$$\frac{\partial z}{\partial x_s} \approx \left. \frac{\partial z}{\partial x_s} \right|_{c=c^*} + \left. \frac{\partial^2 z}{\partial x_s \partial c} \right|_{c=c^*} (c - c^*) + \left. \frac{\partial^3 z}{\partial x_s \partial c^2} \right|_{c=c^*} (c - c^*)^2. \quad (\text{A-1})$$

Differentiating with respect to x_s in equation (5), we have

$$\frac{\partial^2 z}{\partial x_s \partial c} = \frac{z}{c} \frac{\sin 2\theta}{\cos^2(\theta - \phi) \cos^2(\theta + \phi)} \frac{d\theta}{dx_s} + \frac{1}{c} \frac{1}{\cos(\theta - \phi) \cos(\theta + \phi)} \frac{\partial z}{\partial x_s}. \quad (\text{A-2})$$

Nonlinear global optimization migration velocity inversion

when $c=c^*$ (c^* is the real velocity), image depth has no relationship to shot position.

$$\frac{\partial^2 z}{\partial x_s^2} \Big|_{c=c^*} = 0. \quad (\text{A-3})$$

Differentiating with respect to x_s in equation (6), here we suppose x is fixed

$$1 = \frac{-z}{\cos^2(\theta - \phi)} \frac{d\theta}{dx_s} - \tan(\theta - \phi) \frac{\partial z}{\partial x_s}.$$

Differentiating with respect to x_s in the equation above and letting $c=c^*$, we get

$$0 = -z \left(2 \frac{\sin(\theta - \phi)}{\cos^3(\theta - \phi)} \left(\frac{d\theta}{dx_s} \right)^2 + \frac{1}{\cos^2(\theta - \phi)} \frac{d^2\theta}{dx_s^2} \right) \Big|_{c=c^*}. \quad (\text{A-4})$$

Using equation (7), equation (A-4) becomes

$$\frac{d^2\theta}{dx_s^2} = -2 \frac{\sin(\theta - \phi) \cos^3(\theta - \phi)}{z^2} \Big|_{c=c^*}. \quad (\text{A-5})$$

In equation (A-2) let

$$y = \frac{\sin 2\theta}{\cos^2(\theta - \phi) \cos^2(\theta + \phi)}$$

and

$$\begin{aligned} \frac{\partial y}{\partial x_s} &= 2 \frac{\cos 2\theta}{\cos^2(\theta - \phi) \cos^2(\theta + \phi)} \frac{\partial \theta}{\partial x_s} \\ &+ 2 \frac{\sin^2 2\theta}{\cos^3(\theta - \phi) \cos^3(\theta + \phi)} \frac{\partial \theta}{\partial x_s}. \end{aligned} \quad (\text{A-6})$$

Let

$$yy = \frac{1}{c} \frac{1}{\cos(\theta - \phi) \cos(\theta + \phi)},$$

and we get

$$\frac{\partial yy}{\partial x_s} \Big|_{c=c^*} = \frac{\sin 2\theta}{c^* \cos^2(\theta - \phi) \cos^2(\theta + \phi)} \frac{\partial \theta}{\partial x_s}.$$

Differentiating with respect to x_s in equation (A-2), we have

$$\begin{aligned} \frac{\partial^3 z}{\partial x_s^2 \partial c} &= \frac{z}{c} \left(\frac{\partial y}{\partial x_s} \frac{\partial \theta}{\partial x_s} + y \frac{\partial^2 \theta}{\partial x_s^2} \right) \\ &+ \frac{y}{c} \frac{\partial \theta}{\partial x_s} \frac{\partial z}{\partial x_s} + \left(\frac{\partial yy}{\partial x_s} \frac{\partial z}{\partial x_s} + yy \frac{\partial^2 z}{\partial x_s^2} \right). \end{aligned} \quad (\text{A-7})$$

Letting $c=c^*$, we get

$$\frac{\partial^3 z}{\partial x_s^2 \partial c} \Big|_{c=c^*} = \frac{z}{c} \left(\frac{\partial y}{\partial x_s} \frac{\partial \theta}{\partial x_s} + y \frac{\partial^2 \theta}{\partial x_s^2} \right). \quad (\text{A-8})$$

Using equations (A-6), (7), and (A-5), the equation (A-8):

$$\begin{aligned} \frac{\partial^3 z}{\partial x_s^2 \partial c} \Big|_{c=c^*} &= 2 \left(\frac{\cos 2\theta \cos^2(\theta - \phi)}{zc \cos^2(\theta + \phi)} + \frac{\sin^2 2\theta \cos(\theta - \phi)}{zc \cos^3(\theta + \phi)} \right. \\ &\left. - \frac{\sin(\theta - \phi) \sin 2\theta \cos(\theta - \phi)}{cz \cos^2(\theta + \phi)} \right) \Big|_{c=c^*}. \end{aligned} \quad (\text{A-9})$$

From Figure 4, we get

$$\cos(\theta - \phi) = \frac{z}{P_s}. \quad (\text{A-10})$$

$$\frac{\sin 2\theta}{x_r - x_s} = \frac{\cos(\theta + \phi)}{P_s},$$

$$\cos(\theta + \phi) = \frac{z}{P_r}, \text{ i.e. } \sin 2\theta = \frac{z(x_r - x_s)}{P_r P_s}. \quad (\text{A-11})$$

Let w_s denote the horizontal distance from the shot position to x and w_r denote the horizontal distance from x to the receiver position, we have

$$\sin(\theta - \phi) = \frac{w_s}{P_s}, \sin(\theta + \phi) = \frac{w_r}{P_r}. \quad (\text{A-12})$$

and

$$\begin{aligned} \cos 2\theta &= \cos((\theta + \phi) + (\theta - \phi)) \\ &= \cos(\theta + \phi) \cos(\theta - \phi) - \sin(\theta + \phi) \sin(\theta - \phi) \\ &= \frac{z^2}{P_s P_r} - \frac{w_s}{P_s} \frac{w_r}{P_r} = (z^2 - w_s w_r) / (P_s P_r) \end{aligned} \quad (\text{A-13})$$

Using equations (A-11), (A-10), (A-12), and (A-13), equation (A-9) becomes

$$\frac{\partial^3 z}{\partial x_s^2 \partial c} \Big|_{c=c^*} = 2 \left(\frac{(z^2 - w_s w_r) P_r}{zc^* P_s^3} + \frac{P_r (x_r - x_s)^2}{zc^* P_s^3} - \frac{P_r w_s (x_r - x_s)}{c^* z P_s^3} \right). \quad (\text{A-14})$$

Differentiating with respect to c in equation (A-7) and letting $c=c^*$, we have

$$\begin{aligned} \frac{\partial^4 z}{\partial x_s^2 \partial c^2} \Big|_{c=c^*} &= - \left(\frac{\partial y}{\partial x_s} \frac{\partial \theta}{\partial x_s} + y \frac{\partial^2 \theta}{\partial x_s^2} \right) \left(\frac{z}{c^2} - \frac{1}{c} \frac{\partial z}{\partial c} \right) \\ &+ \frac{y}{c} \frac{\partial \theta}{\partial x_s} \frac{\partial^2 z}{\partial x_s \partial c} + \left(\frac{\partial yy}{\partial x_s} \frac{\partial^2 z}{\partial x_s \partial c} + yy \frac{\partial^3 z}{\partial x_s^2 \partial c} \right), \end{aligned}$$

let

$$D_1 = - \left(\frac{\partial y}{\partial x_s} \frac{\partial \theta}{\partial x_s} + y \frac{\partial^2 \theta}{\partial x_s^2} \right) \left(\frac{z}{c^2} - \frac{1}{c} \frac{\partial z}{\partial c} \right),$$

$$D_2 = \frac{\partial yy}{\partial x_s} \frac{\partial^2 z}{\partial x_s \partial c} + yy \frac{\partial^3 z}{\partial x_s^2 \partial c}, \quad D_3 = \frac{y}{c} \frac{\partial \theta}{\partial x_s} \frac{\partial^2 z}{\partial x_s \partial c},$$

and

$$\frac{\partial^4 z}{\partial x_s^2 \partial c^2} \Big|_{c=c^*} = D_1 + D_2 + D_3.$$

Using equation (5), we get

$$D_1 = -\frac{1}{c} \frac{\partial^3 z}{\partial x_s^2 \partial c} \left(1 - \frac{1}{\cos(\theta - \phi) \cos(\theta + \phi)} \right) \Big|_{c=c^*}.$$

Using equation (A-14), we have

$$\begin{aligned} D_1 = & -\frac{2}{c^*} \left(\frac{(z^2 - w_s w_r) P_r}{z c^* P_s^3} + \frac{P_r (x_r - x_s)^2}{z c^* P_s^3} \right. \\ & \left. - \frac{P_r w_s (x_r - x_s)}{c^* z P_s^3} \right) \left(1 - \frac{P_s P_r}{z^2} \right), \\ D_2 = & 2 \frac{\sin 2\theta}{c^* \cos^2(\theta - \phi) \cos^2(\theta + \phi)} \frac{\partial^2 z}{\partial x_s \partial c} \\ & + \frac{1}{c^*} \frac{1}{\cos(\theta - \phi) \cos(\theta + \phi)} \frac{\partial^3 z}{\partial x_s^2 \partial c}. \end{aligned} \quad (\text{A-15})$$

Substituting equation (A-10), (A-11), and (A-14), we have

$$\begin{aligned} D_2 = & 2 \frac{P_r^2 (x_r - x_s)^2}{c^{*2} z^4} + 2 \frac{P_s P_r}{c z^2} \left(\frac{(z^2 - w_s w_r) P_r}{z c^* P_s^3} \right. \\ & \left. + \frac{P_r (x_r - x_s)^2}{z c^* P_s^3} - \frac{P_r w_s (x_r - x_s)}{c^* z P_s^3} \right), \end{aligned}$$

and

$$D_3 = -\frac{1}{c z} \frac{\sin 2\theta}{\cos^2(\theta + \phi)} \frac{\partial^2 z}{\partial x_s \partial c}.$$

Using equations (A-10) and (A-11), we get

$$D_3 = \frac{1}{c^{*2} z^3} \frac{(x_r - x_s)^2 P_r^2}{P_s^2}.$$

Expanding $\frac{\partial^2 z}{\partial x_s^2}$ at $c = c^*$ to quadratic terms of the Taylor series, yields

$$\frac{\partial^2 z}{\partial x_s^2} \approx \frac{\partial^2 z}{\partial x_s^2} \Big|_{c=c^*} + \frac{\partial^3 z}{\partial x_s^2 \partial c} \Big|_{c=c^*} (c - c^*) + \frac{\partial^4 z}{\partial x_s^2 \partial c^2} \Big|_{c=c^*} (c - c^*)^2 \quad (\text{A-16})$$

Using equation (A-3), (A-14), and (A-16), equation (A-7) becomes

$$\begin{aligned} \frac{\partial^2 z}{\partial x_s^2} \approx & 2 \left(\frac{(z^2 - w_s w_r) P_r}{z c^* P_s^3} + \frac{P_r (x_r - x_s)^2}{z c^* P_s^3} - \frac{P_r w_s (x_r - x_s)}{c^* z P_s^3} \right) (c - c^*) \\ & + (D_1 + D_2 + D_3) (c - c^*)^2. \end{aligned} \quad (\text{A-17})$$

Let

$$D_0 = 2 \left(\frac{(z^2 - w_s w_r) P_r}{z c^* P_s^3} + \frac{P_r (x_r - x_s)^2}{z c^* P_s^3} - \frac{P_r w_s (x_r - x_s)}{c^* z P_s^3} \right).$$

Simplifying the equation above, we have

$$\frac{\partial^2 z}{\partial x_s^2} \approx D_0 (c - c^*) + (D_1 + D_2 + D_3) (c - c^*)^2. \quad (\text{A-18})$$

Suppose that we have three shots: x_{s1} , x_{s2} , and x_{s3} , and $x_{s1} < x_{s2} < x_{s3}$, the imaged depth difference in CIG can be approximated by

$$\frac{\partial z(x_{s23})}{\partial x_s} - \frac{\partial z(x_{s12})}{\partial x_s} \approx \frac{\partial^2 z(x_{s13})}{\partial x_s^2} (x_{s3} - x_{s1}) / 2, \quad (\text{A-19})$$

and

$$\frac{z(x_{s3}) - z(x_{s2})}{x_{s3} - x_{s2}} - \frac{z(x_{s2}) - z(x_{s1})}{x_{s2} - x_{s1}} \approx \frac{\partial^2 z(x_{s13})}{\partial x_s^2} (x_{s3} - x_{s1}) / 2, \quad (\text{A-20})$$

where

$$x_{s12} = (x_{s1} + x_{s2}) / 2, \quad x_{s23} = (x_{s2} + x_{s3}) / 2,$$

and

$$x_{s13} = (x_{s3} + x_{s1}) / 2,$$

Using equation (A-18), equation (A-20) can become

$$\begin{aligned} & 2 \left(\frac{z(x_{s3}) - z(x_{s2})}{x_{s3} - x_{s2}} - \frac{z(x_{s2}) - z(x_{s1})}{x_{s2} - x_{s1}} \right) / (x_{s3} - x_{s1}) \\ & \approx D_0 (c - c^*) + (D_1 + D_2 + D_3) (c - c^*)^2. \end{aligned} \quad (\text{A-21})$$

For simplification, let: $A_2 = D_1 + D_2 + D_3$

$$A_1 = D_0,$$

and

$$A_0 = 2 \left(\frac{z(x_{s3}) - z(x_{s2})}{x_{s3} - x_{s2}} - \frac{z(x_{s2}) - z(x_{s1})}{x_{s2} - x_{s1}} \right) / (x_{s3} - x_{s1}).$$

Using equations A_2 , A_1 , and A_0 , equation (A-21) becomes

$$A_0 = A_1 (c - c^*) + A_2 (c - c^*)^2. \quad (\text{A-22})$$

Zhao Taiyin is a Ph. D. student at University of Electronic



Science and Technology of China (UESTC). Graduated and received a Master degree in Solid Geophysics from Chengdu University of Technology in 2002. He is interested in seismic signal processing, imaging and migration velocity analysis.

计算公式由于包含有速度横向导数项,在速度横向变化大的介质中,也能有较高的聚焦效果,而且也走时计算提供了精确的相对振幅保持系数。本文对推导的方法进行模型测试并进行实际数据的试算,其结果证明非对称走时方法的成像精度远高于对称走时计算方法。

关键词: 单程波算子, 走时公式, 李代数, 拟微分算子

二阶精度广义非线性全局最优的偏移速度反演方法 // A quadratic precision generalized nonlinear global optimization migration velocity inversion method, 赵太银¹, 胡光岷¹, 贺振华², 黄德济², APPLIED GEOPHYSICS, 6(2), P. 138 - 149

(1. 电子科技大学通信与信息工程学院, 成都 610054; 2. 成都理工大学油气藏地质与开发工程国家重点实验室, 成都 610059)

摘要: 如何快速、精确地利用叠前深度偏移进行偏移速度分析是勘探地震学的一项重要研究内容,针对该问题,本文提出一种二阶精度广义非线性全局最优的偏移速度反演方法。我们将首先去掉速度模型修正量与成像深度呈线性关系的假设,推导出具有二阶精度的速度模型修正量计算公式,使每一次迭代得到的速度模型尽可能地接近实际模型;然后采用广义非线性反演方法反演获得对所有道集的全局最优的速度模型修正量,不仅极大地加快了收敛速度,而且反演过程中陷入局部极小的可能性也减小了。理论模型和Marmousi模型的处理结果表明:本方法精度高、处理速度快,提高了偏移速度分析方法的实用性和对复杂构造成像的准确性。

关键词: 叠前深度偏移, 偏移速度分析, 广义非线性反演, 共成像道集

零偏VSP资料波阻抗反演方法研究 // Acoustic impedance inversion of zero-offset VSP data, 王静^{1,2}, 刘洋^{1,2}, 孙哲^{1,2}, 田洪³, 苏华³, 赵前华³, 刘颖宇³, APPLIED GEOPHYSICS, 6(2), P. 150 - 158

(1. 中国石油大学(北京)油气资源与探测国家重点实验室, 北京 102249; 2. 中国石油大学(北京)CNPC物探重点实验室, 北京 102249; 3. 中海油田服务股份有限公司油田技术事业部, 河北, 燕郊 065201)

摘要: VSP资料钻前预测的关键在于高精度的波阻抗反演,本文针对VSP资料高分辨率、高信噪比以及能精确地分离出上、下行波的特点,提出了一种利用VSP资料进行井底以下钻头前方地层波阻抗反演的方法。该方

法首先对VSP走廊叠加记录采用非线性迭代反演方法反演地下地层的波阻抗;通过在迭代过程中不断修改阻尼因子,以及引入预条件共轭梯度法求解方程组,增强了解的稳定性和收敛速度。理论模型与实际资料的处理结果表明该方法具有较好的效果,并在VSP资料钻前预测研究中具有良好的应用前景。

关键词: 零偏VSP, 波阻抗反演, 非线性迭代反演, 阻尼因子, 预条件共轭梯度法

高分辨率非线性三维整体反演研究 // High resolution 3D nonlinear integrated inversion, 李勇¹, 王绪本¹, 李志荣², 李琼¹, 李正文¹, APPLIED GEOPHYSICS, 6(2), P. 159 - 165

(1. 成都理工大学“地球探测与信息技术”教育部重点实验室, 成都 610059; 2. 川庆钻探工程公司地球物理勘探公司, 成都 610213)

摘要: 高分辨率非线性三维整体反演方法是基于非线性理论,在层位控制下,将工区多井(或全部井)的测井数据与井旁地震道数据输入具有多输入多输出的网络,同时进行整体训练,可获得整个工区的自适应权函数,并建立综合非线性映射关系,并根据储层在纵横方向上的地质变化特征更新这种非线性映射关系,这样,就能对反演过程及其反演结果起到约束和控制的作用,从而获得稳定且分辨率高的地震反演剖面(速度反演剖面/波阻抗反演剖面/密度反演剖面),实现整体反演,该方法通过模型试算和实际资料处理,获得较好的地质效果,证明该方法精度高、实用性强,可用于储层的定量分析。

关键词: 高分辨率, 整体反演, 多输入多输出网络, 混合智能学习算法

地球物理资料群体智能反演 // Swarm intelligence optimization and its application in geophysical data inversion, 袁三一, 王尚旭, 田楠, APPLIED GEOPHYSICS, 6(2), P. 166 - 174

(中国石油大学CNPC物探重点实验室, 北京 102249)

摘要: 复杂地球物理资料的反演问题往往是一个求解多参数非线性多极值的最优解问题。而鸟和蚂蚁等群体觅食的过程,正好与寻找地球物理反演最优解的过程相似。基于自然界群体协调寻优的思想,本文提出了交叉学科的群体智能地球物理资料反演方法,并给出了其对应的数学模型。用一个有无限多个局部最优解的已知模型对该类方法进行了试验。然后,将它们应用到了不同的复杂地球物理反演问题中:(1)对噪声敏感的线性问题;(2)非线性和线性同步反演问